Light-emitting ambipolar organic heterostructure field-effect transistor

Rost, Constance; Karg, Siegfried; Riess, Walter; Loi, Maria Antonietta; Murgia, Mauro; Muccini, Michele

Published in:
Synthetic Metals

DOI:
10.1016/j.synthmet.2004.08.003

Publication date:
2004

Available online at www.sciencedirect.com
SCIENCE DIRECT®
Synthetic Metals 146 (2004) 237–241
SYNTHETIC METALS
www.elsevier.com/locate/synmet

Light-emitting ambipolar organic heterostructure field-effect transistor

Constance Rost[a,*], Siegfried Karg[a], Walter Riess[a], Maria Antonietta Loi[b], Mauro Murgia[b], Michele Muccini[b]

[a] *IBM Research GmbH, Säumerstrasse 4, CH-8803 Rüschlikon, Switzerland*
[b] *Consiglio Nazionale delle Ricerche - Istituto per lo Studio dei Materiali Nanostrutturati (CNR-ISMN), via P. Gobetti 101, 40129 Bologna, Italy*

Available online 15 September 2004

Abstract

We have investigated ambipolar charge injection and transport in organic field-effect transistors (OFETs) as prerequisites for a light-emitting organic field-effect transistor (LEOFET). OFETs containing a single material as active layer generally function either as a p- or an n-channel device. Therefore, ambipolar device operation over a wide range of operating voltages is difficult to realize. Here, we present a highly asymmetric heterostructure OFET architecture using the hole transport material pentacene and the electron transport material *N*,*N*′-ditridecylperylene-3,4,9,10-tetracarboxylic diimide (PTCDI-$C_{13}H_{27}$). Efficient charge carrier injection is achieved by using Au as bottom contact for hole injection into pentacene and Mg as top contact for electron injection into PTCDI-$C_{13}H_{27}$. The device characteristic of this asymmetric heterostructure shows all features of ambipolar operation. For example, a typical transistor characteristic with a linear and saturation region is observed for small drain-source voltage V_{DS}. For large V_{DS}, the current increases due to additional injection of charge carriers of opposite sign from the drain contact. In that regime, both types of charge carriers are present in the device. Thus, the thin-film transistor can be operated in a mixed state in which both electron and hole currents are transported within the device and where the double injection regime is controlled by the gate voltage. Our device exhibits electron and hole mobilities of 3×10^{-3} cm^2/Vs and 1×10^{-4} cm^2/Vs, respectively. Investigation of a bulk heterostructure of a thienylene derivative and PTCDI-$C_{13}H_{27}$ results in a light-emitting field-effect transistor. The light emission is controlled by both the drain-source voltage V_{DS} and the gate voltage V_G.

Keywords: Light-emitting; Ambipolar; Transistor

1. Introduction

Electronic thin-film devices based on organic materials are extensively investigated in the form of organic light-emitting diodes (OLEDs) [1,2], organic solar cells [3,4], electro-chemical cells [5] and organic field-effect transistors (OFETs) [6–9]. The progress in the field of OLEDs for display applications was recently highlighted by the demonstration of a 20-in. full-color active-matrix OLED display, driven by amorphous Si thin-film transistors [10]. OFETs are being developed as switching devices for active-matrix OLED displays [11] and for low-cost electronics, such as low-end smart cards and electronic identification tags. Combining light emission with switching characteristics in a single device, i.e., a light-emitting field-effect transistor (LEFET), would not only increase the number of potential applications of organic optoelectronic devices, but also present an ideal structure for lifetime studies of organic light-emitting materials under different driving conditions and charge-carrier balances. Similar to an OLED, light emission from an OFET requires electron and hole injection and transport as well as exciton formation followed by efficient radiative decay. Ambipolar device characteristics have been observed and described in detail in amorphous silicon field-effect transistors (FETs) [12–14]. However, in organic materials typically unipolar transport is observed, i.e., one type of charge carrier is transported preferably, and thus, the transistor operates either as a p- or an n-channel device. This is even the case for single-material LEOFETs [15–17]. In order to overcome

* Corresponding author. Tel.: +41 1 724 8272; fax: +41 1 724 8956.
E-mail address: cro@zurich.ibm.com (C. Rost).

0379-6779/$ – see front matter © 2004 Elsevier B.V. All rights reserved.
doi:10.1016/j.synthmet.2004.08.003

this problem, we have investigated heterostructures of organic hole and electron transport materials. Here we report ambipolar field effect transistors based on pentacene as hole transport material and PTCDI-$C_{13}H_{27}$ as electron transport material [18]. Concerning light emission, an ambipolar light-emitting transistor would allow the electron-hole balance as well as the location of the recombination zone between source and drain electrodes to be tuned by the gate voltage. In order to achieve light emission from an ambipolar field-effect transistor, we have replaced the hole transport material pentacene with a thienylene derivative.

2. Device preparation and experimental methods

We fabricated OFET devices using pentacene as the hole-transport material and *N,N*-ditridecylperylene-3,4,9,10-tetracarboxylic diimide (PTCDI-$C_{13}H_{27}$) as the electron-transport material in a heterostructure. Pentacene is a thoroughly investigated hole-transport material, for which a hole mobility of up to 2.2 cm^2/Vs has been reported [19]. PTCDI-$C_{13}H_{27}$ belongs to a class of perylene derivatives, which are well-studied electron-transport materials. For a similar compound, PTCDI-C_8H_{17}, which differs only in its shorter C_8H_{17} side chain, an electron mobility of up to 0.6 cm^2/Vs has been reported [20]. The schematic architecture of our device is shown in Fig. 1(a). A heavily doped, n-type Si wafer (doping level 10^{18}/cm^3) with an aluminum back contact acts as gate electrode and substrate. The gate insulator consists of a thermally grown SiO2 layer with a thickness of 150 nm. Prior to processing, the oxidized wafer was cleaned with a standard wet cleaning procedure, comprising ultrasonic cleaning in acetone and isopropanol. In order to achieve efficient hole and electron injection, we incorporate Au and Mg as electrodes with high and low work functions, respectively, resulting in source and drain contacts with low injection barriers. The Au contact was thermally evaporated in a high-vacuum chamber at a pressure of 5×10^{-7} mbar and had a thickness of 40 nm; its lateral dimensions were defined by shadow masks. Next, the organic heterostructure was evaporated, starting with a pentacene film (30 nm) followed by a PTCDI-$C_{13}H_{27}$ film (50 nm). The deposition rate was typically 0.5 Å/s. Finally, the 50-nm thick Mg top contact was evaporated through a second shadow mask. The completed device structure represents a highly asymmetric FET with respect to source and drain contacts and both active organic layers (Fig. 1(a)). The channel length and width of the heterostructure OFET were 140 and 2000 μm, respectively. The preparation of the bulk heterostructure device consisting of PTCDI-$C_{13}H_{27}$ and the thienylene derivative is described elsewhere [21]. The energetic levels of the highest occupied molecular orbital (HOMO) and the lowest unoccupied molecular orbital (LUMO) of pentacene and of PTCDI-$C_{13}H_{27}$ with respect to the work function of Au and Mg are shown schematically in Fig. 1(b). The HOMO level of pentacene lies at 5.0 eV [22] and is aligned with the work function of Au at 5.1 eV [23], resulting in an efficient injection of holes into the pentacene layer. Mg with its work function of 3.7 eV [23] is chosen as electron-injecting contact to reduce the barrier for electron injection into the PTCDI-$C_{13}H_{27}$ LUMO level at 3.4 eV. The values for the relevant energy levels of PTCDI-$C_{13}H_{27}$ were estimated from [24]. For characterization, the devices were transferred through air into an argon glove box (<1 ppm O_2, H_2O). The transistor output and transfer characteristics were measured with a probe station using an Agilent 4155C semiconductor parameter analyzer. Simultaneously, the electroluminescence (EL) intensity was measured using a Hamamatsu S1336 photodiode. The charge-carrier mobility can be extracted from the transfer characteristics using the saturated drain current $I_{D,sat}$ versus V_G relation

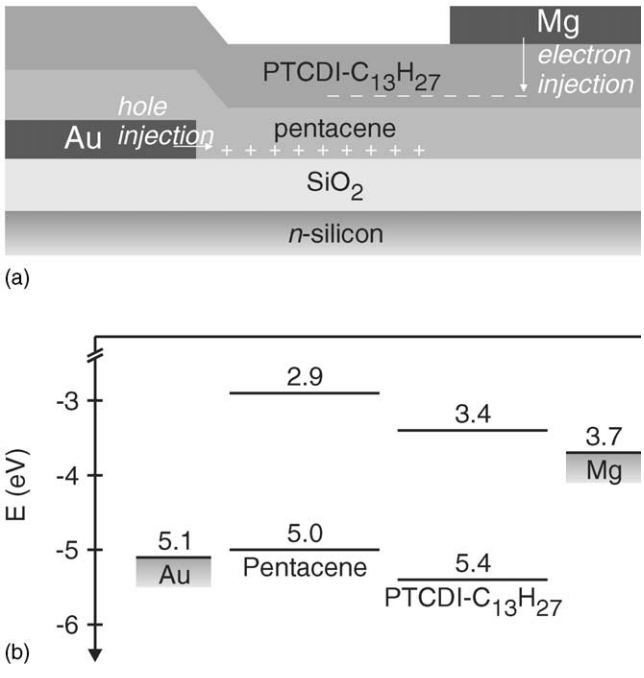

Fig. 1. (a) Device structure of the field-effect transistor based on an organic heterostructure. Shown is the schematic p- and n-channel formation to illustrate the field-induced charge distribution under negative gate-source voltage V_G and drain-source voltage V_{DS}, with $|V_{DS}| > |V_G|$. (b) Energy levels (HOMO and LUMO) of pentacene [22] and PTCDI-$C_{13}H_{27}$ and work function of the two metal contacts, Au and Mg [23]. The values for PTCDI-$C_{13}H_{27}$ were estimated from [24]. Reprinted with permission from [18].

$$I_{D,sat} = \frac{W}{2L}\mu C(V_G - V_T)^2 \quad (1)$$

Here, W stands for the channel width, L for the channel length, μ for the charge carrier mobility, C for the gate-oxide capacitance per unit area, V_G for the gate voltage and V_T for the threshold voltage. The value of V_T is derived from the intersection of the linear slope of the square root of $I_{D,sat}$ versus V_G with the abscissa. The current on–off ratio is obtained from the semi-logarithmic plot of $I_{D,sat}$ versus V_G.

3. Results and discussion

Fig. 2 shows the output characteristics of a heterostructure transistor. As the device architecture itself is asymmetric with respect to the source and drain electrodes and the two organic layers, it is important to differentiate not only between positive and negative gate bias, but also between the two cases of either Au or Mg being defined as source contact. Applying a negative gate bias V_{GS} with respect to the Au electrode, typical p-channel characteristics are observed for negative drain-source voltages with $|V_{DS}| \lesssim |V_G|$. In this voltage range, p-channel characteristics originate from an accumulation layer of holes formed at the pentacene/SiO_2 interface. By increasing $|V_{DS}|$ above a certain value that is gate-bias-dependent (we obtain the following empirical relation: $|V_{DS}| \gtrsim |V_G| + |V_T|$ with $V_T \simeq -10$ V), an abrupt, steep increase in the current is measured. Such a steep increase in the channel current is a typical characteristic of ambipolar operation in OFETs (see also [25] and [26]). In this voltage range with $|V_{DS}| \gtrsim |V_G| + |V_T|$, the gate contact is biased positive with respect to the drain contact. As the Mg contact energetically favors electron injection into PTCDI-$C_{13}H_{27}$, an accumulation layer of electrons is expected to form in the PTCDI-$C_{13}H_{27}$ layer on top of the pentacene layer. Therefore, the current increase is attributed to the injection of electrons into the PTCDI-$C_{13}H_{27}$ layer and the transport of electrons in a channel formed close to the pentacene layer.

Considering the transistor output characteristics, with the Mg contact defined as source (common) under positive gate bias. For $V_G \geq 15$ V, we observe typical n-channel characteristics. As expected for normal transistor output characteristics, the magnitude of I_D increases with increasing V_G. The current is due to electrons that are injected from the Mg contact into the PTCDI-$C_{13}H_{27}$ layer and expected to be transported adjacent to the pentacene layer. However, for $V_G \leq 10$ V, we again observe the pronounced increase of

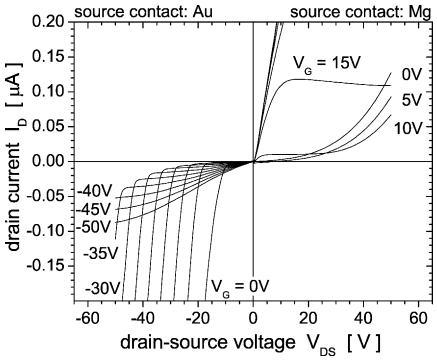

Fig. 2. Output characteristics of the heterostructure transistor. I_D was measured for negative and positive values of V_G and V_{DS}. The bias was applied versus the Au and the Mg contact, respectively. In both cases, transistor characteristics are observed with a saturation region for the p-channel regime as well as for the n-channel regime. The other type of charge carrier is injected for large drain-source voltages, resulting in ambipolar transport, observed as a pronounced increase of the drain current. Adapted with permission from [18].

I_D with for large values of V_{DS}. The current increases with decreasing V_G, and no current saturation is measured for $V_G \leq 5$ V. In this voltage regime, the gate contact is negatively biased with respect to the drain contact and therefore, the nonsaturating current originates from holes injected from the Au contact into the pentacene layer.

The ambipolar current originates from both types of charge carriers. Regardless of whether we are in the positive or negative bias regime, one of these currents saturates, whereas for the other no saturation can be observed. In the heterostructure transistor, we therefore always measure a superposition of both the saturating and the nonsaturating characteristics, independent of the voltage regime (positive or negative bias) we are in. Simple modeling of the ambipolar characteristics using the Shockley model [27,28] for unipolar OFETs, summing up the electron and hole currents, and taking the estimated threshold voltages into account, electron and hole mobilities of 3×10^{-3} cm^2/Vs and 1×10^{-4} cm^2/Vs can be derived, respectively. Even though pentacene exhibits a relatively high hole mobility in single-layer devices, the mobility in the heterostructure transistor is much lower. This could be due to morphology changes in the pentacene film caused by the second organic layer. Additionally, it is not clear whether Eq. (1) can still be used because the effective gate voltage applied to the device could be significantly influenced by the heterostructure. Theoretical studies to clarify this are underway, and will be published elsewhere.

Light emission depends strongly on the relative positions of the energy levels of the HOMO and the lowest LUMO of the two organic semiconductors. In that respect, pentacene is not the most suitable material for light emission. In field-effect devices based on bulk heterostructures, i.e. devices with a coevaporated layer rather than a bilayer, of PTCDI-$C_{13}H_{27}$ and a wide-band-gap thienylene derivative, light emission can be observed [21].

Fig. 3(a) shows the output characteristics of a transistor with such a bulk heterostructure. Applying a negative gate bias V_G, typical p-channel characteristics are observed in the third quadrant for negative drain-source voltages with $|V_{DS}| \leq |V_G|$. With increasing $|V_{DS}|$, an abrupt, steep increase in the drain current I_D is measured, which is a typical characteristic of ambipolar operation in OFETs (see also [25,26]). This current increase is attributed to the injection of electrons into the organic thin film at the drain contact. A similar behavior is observed for positive gate bias in the first quadrant. The most striking feature, however, is the light emission monitored by the photocurrent of the photodiode as shown in Fig. 3(b). For negative drain-source and gate voltages, the light output is apparently correlated to the nonsaturating drain current. The highest brightness is achieved for $V_G = 0$ V and $V_{DS} = -50$ V. For positive drain-source voltages, only weak emission is observed. In contrast to the negative-voltage case, the emission occurs at high gate voltages.

The light output from an ambipolar device is proportional to the recombination rate of electrons and holes between

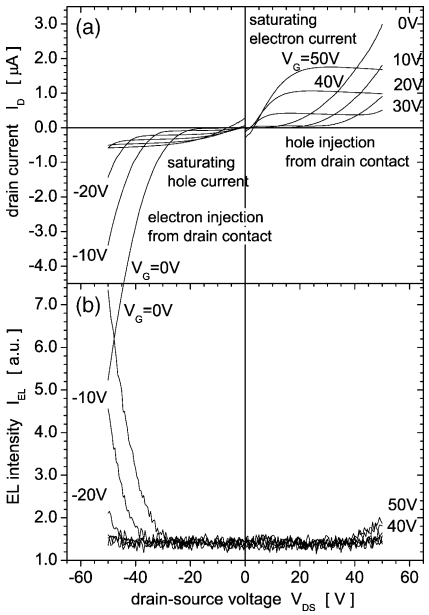

Fig. 3. (a) Output characteristics and (b) light intensity for the bulk heterostructure thin-film transistor for negative and positive gate bias. Adapted with permission from [21].

source and drain electrode. Assuming Langevin recombination [29], the EL intensity I_{EL} is

$$I_{EL} \propto \int_0^L \frac{e}{\varepsilon_r \varepsilon_o}(\mu_n(x) + \mu_p(x))n(x)p(x)d(x) \quad (2)$$

where ε_r is the dielectric constant of the bulk-heterojunction organic layer, n(x) and p(x) are the electron and hole densities, and $\mu_n(x)$ and $\mu_p(x)$ are the electron and hole mobilities along the channel, respectively. Whereas the drain current I_D is a superposition of the electron and the hole current, the light intensity is determined by the n(x)p(x) product. Therefore, no simple correlation of drain current and EL intensity seems to exist. A quantitative description of the ambipolar drain current, the hole and electron densities along the channel, and the light output will be given elsewhere [30].

Fig. 4 shows the transfer characteristics of the device. For large $|V_G|$, the current originates either from holes for negative values of V_G or from electrons for positive values of V_G. The square root of the drain current I_D shows the expected linear dependence on V_G, as is known from unipolar devices. Contrary to unipolar devices, where a continuous increase in drain current $|I_D|$ is typically observed for absolute increasing gate voltage $|V_G|$, we observe first a decrease in $|I_D|$ for small values of $|V_G|$, which only starts to increase again after a certain value of $|V_G|$. This current originates from the corresponding opposite type of charge carrier. For increasing drain-source voltages, the minimum in drain current shifts towards larger gate voltages. From the linear slope of the square root of I_{DS} versus V_G, a hole mobility of 10^{-4} cm^2/Vs and an electron mobility of 10^{-3} cm^2/Vs can be extracted.

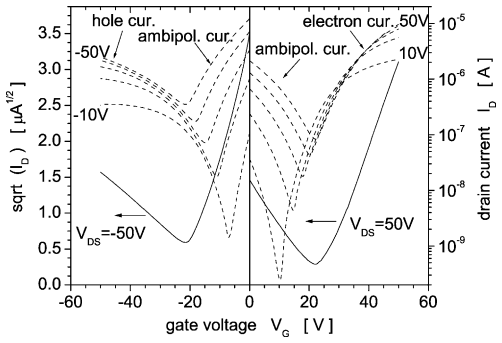

Fig. 4. Transfer characteristics of the bulk heterostructure thin-film transistor for negative and positive gate bias. The solid lines show the square root of the drain current, the dashed lines the logarithmic drain-current vs. gate voltage for various drain-source voltages V_{DS}. Reprinted with permission from [21].

4. Conclusion

We have demonstrated OFETs based on organic heterostructures that exhibit ambipolar conduction over a wide range of bias conditions. Depending on the applied gate bias, either an accumulation layer of holes (negative gate bias) is formed in the pentacene layer or an accumulation layer of electrons (positive gate bias) is formed in the PTCDI-$C_{13}H_{27}$ layer of the heterostructure device. By applying an additional drain-source voltage, wheras for other bias conditions, it is predominantly a p-channel device. There are even bias regimes in which accumulation layers for both carrier types are formed close to the corresponding contacts, and charge carriers of both polarities can be simultaneously injected from the source and the drain contact. The device has been designed such that it allows the formation of two accumulation layers, one for holes within the pentacene layer, the other for electrons within the PTCDI-$C_{13}H_{27}$ layer. This is possible by offsetting the energy levels of pentacene and PTCDI-$C_{13}H_{27}$ in such a way that energetic barriers prevent the charges from flowing into the other material (Fig. 2). The source and drain electrodes are tailored for efficient carrier injection by choosing the high-work-function metal Au for hole injection and the low-work-function metal Mg for electron injection.

Bulk heterostructures of a wide band gap hole transport material and PTCDI-$C_{13}H_{27}$ lead to LEOFETs that exhibit pronounced ambipolar conduction over a wide range of bias conditions accompanied by light emission. Light emission is controlled by the drain current, and can be modulated by both the drain-source voltage and the gate voltage. Therefore, the device serves as an excellent model structure for a LEOFET.

Acknowledgments

This work is funded within the EU-IST-FET program under project IST-33057 (ILO). The authors thank Th. Linder and G. Paasch (IFW Dresden) for useful discussions, and M. Melucci and G. Barbarella (CNR-ISOF Bologna) for

providing α-5T. The authors acknowledge T. Beierlein, U. Drechsler, H. Riel, M. Tschudy (IBM ZRL) and R. Zamboni (CNR-ISMN Bologna) for support.

References

[1] C.W. Tang, S.A. VanSlyke, Appl. Phys. Lett. 51 (1987) 913.
[2] R.H. Friend, R.W. Gymer, A.B. Holmes, J.H. Burroughes, R.N. Marks, C. Taliani, D.D.C. Bradley, D.A. Dos Santos, J.L. Brédas, M. Lögdlund, W.R. Salaneck, Nature 397 (1999) 121.
[3] S.E. Shaheen, C.J. Brabec, N.S. Sariciftci, F. Padinger, T. Fromherz, J.C. Hummelen, Appl. Phys. Lett. 78 (2001) 841.
[4] P. Peumans, S. Uchida, S.R. Forrest, Nature 425 (2003) 158.
[5] L. Edman, M. Pauchard, B. Liu, G. Bazan, D. Moses, A.J. Heeger, Appl. Phys. Lett. 82 (2003) 3961.
[6] K. Kudo, M. Yamashina, T. Moriizuni, Jpn. J. Appl. Phys. 23 (1984) 130.
[7] G. Horowitz, D. Fichou, X. Peng, Z. Xu, F. Garnier, Solid State Commun. 72 (1989) 381.
[8] D.J. Gundlach, Y.Y. Lin, T.N. Jackson, S.F. Nelson, D.G. Schlom, IEEE Electron. Device Lett. 18 (1997) 87.
[9] H. Sirringhaus, N. Tessler, R.H. Friend, Science 280 (1998) 1741.
[10] T. Tsujimura, in SID 2003 Technical Digest, vol. XXXIV, Book 1, 2003, pp. 6.
[11] T.N. Jackson, Y.Y. Lin, D.J. Gundlach, H. Klauk, IEEE J. Sel. Top. Quantum Electron. 4 (1998) 100.
[12] H. Pfleiderer, W. Kusian, Solid-State Electron. 29 (1986) 317.
[13] H. Pfleiderer, IEEE Trans. Electron. Device 33 (1986) 145.
[14] G.W. Neudeck, H.F. Bare, K.Y. Chung, IEEE Trans. Electron. Device 34 (1987) 344.
[15] A. Hepp, H. Heil, W. Weise, M. Ahles, R. Schmechel, H. von Seggern, Phys. Rev. Lett. 91 (2003) 157406.
[16] C. Santato, R. Capelli, M.A. Loi, M. Murgia, F. Cicoira, V.A.L. Roy, P. Stallinga, R. Zamboni, C. Rost, S.F. Karg, M. Muccini, Synthetic Metals (in press).
[17] R. Capelli, M.A. Loi, C. Santato, and M. Muccini, Organic Electronics (submitted for publication).
[18] C. Rost, D.J. Gundlach, S. Karg, W. Riess, J. Appl. Phys. 95 (2004) 5782.
[19] Y.-Y. Lin, D.J. Gundlach, S.F. Nelson, T.N. Jackson, IEEE Trans. Electron. Device 44 (1997) 1325.
[20] P.R.L. Malenfant, C.D. Dimitrakopoulos, J.D. Gelorme, A. Curioni, W. Andreoni, Appl. Phys. Lett. 80 (2002) 2517.
[21] C. Rost, S. Karg, and W. Riess, M.A. Loi, M. Murgia, and M. Muccini, Appl. Phys. Lett. 85 (2004) 1613.
[22] N. Karl, in: R. Farchioni, G. Grosso (Eds.), Organic Electronic Materials, Springer Series in Materials Science, vol. 41, Springer-Verlag, Berlin Heidelberg, New York, 2001, pp.
[23] CRC Handbook of Chemistry and Physics, 77th edition, CRC Press, Boca Raton, 1996.
[24] M. Hiramoto, K. Ihara, H. Fukusumi, M. Yokohama, J. Appl. Phys. 78 (1995) 7153.
[25] E.J. Meijer, D.M. de Leeuw, S. Estalles, E. van Veenendaal, B.-H. Huisman, P.W.M. Blom, J.C. Hummelen, U. Scherf, T.M. Klapwijk, Nat. Mater. 2 (2003) 678.
[26] A. Dodabalapur, H.E. Katz, L. Torsi, R.C. Haddon, Appl. Phys. Lett. 68 (1996) 1108.
[27] S.M. Sze, Physics of Semiconductor Devices, John Wiley, New York, 1981.
[28] G. Horowitz, Adv. Mater. 10 (1998) 365.
[29] M.A. Lampert, P. Mark, Current Injection in Solids, Academic Press, New York, 1970.
[30] Th. Lindner, G. Paasch, C. Rost, S. Karg, W. Riess, in preparation.